Revista Mexicana de Astronomía y Astrofísica, **36**, 57–66 (2000)

THE EFFECT OF PISTON ERRORS ON THE IMAGE QUALITY OF GROUND-BASED SEGMENTED MIRROR TELESCOPES

C. D. Bello

Instituto de Astrofísica de Canarias, Spain

N. Devaney and J. Castro

Gran Telescopio Canarias, Spain

Received 1999 October 20; accepted 2000 March 8

RESUMEN

Los errores asociados con un espejo primario segmentado limitan la calidad de imagen alcanzable con aquellos telescopios que los utilicen. Es necesario derivar los efectos de los errores propios de la segmentación en la calidad de imagen, de forma que se puedan elaborar presupuestos de errores realistas para dichos telescopios. La mayor parte de los errores de segmentación son el desalineado y pistón de los segmentos, así como los errores de figura. En este trabajo el efecto de la segmentación en la calidad de imagen se estudia analíticamente considerando un telescopio con un espejo primario formado por dos anillos. Derivamos expresiones aproximadas para la MTF y CIR (cociente de intensidad central) siguiendo la técnica descrita por Dierickx (1992). Mediante simulaciones numéricas se prueba que los resultados pueden aplicarse a telescopios con esquemas de segmentación realistas, con errores de pistón de hasta $\approx$ 80nm.

ABSTRACT

The errors associated with a segmented primary mirror limit the image quality obtainable with those astronomical telescopes which employ them. It is necessary to derive the effects of segmentation errors on image quality in order to determine realistic error budgets for such telescopes. The main segmentation errors are misalignment and piston of the segments as well as figure errors. Here, the effect of segmentation on image quality is studied analytically by considering a two-ring telescope. Approximate expressions for the MTF and CIR (Central Intensity Ratio) are derived following the technique described by Dierickx (1992). It is found by numerical simulation that the results may be applied to telescopes with realistic segmentation schemes for piston errors up to $\approx$ 80nm.

Key words: **METHOD: ANALYTICAL — TELESCOPES**

1. INTRODUCTION

Modern observational astronomy demands telescopes with ever-increasing collecting areas. At the same time, it is required that these telescopes have superb image quality, in order not to degrade the excellent *seeing* conditions which frequently occur at mountaintop observatories. The 8m-class telescopes currently under construction appear to be at the limit of monolithic mirror technology. In order to construct larger telescopes, it will be necessary to employ segmented mirrors. Indeed, the largest telescopes in the world already employ segmented primary mirrors (Nelson & Gillingham 1994; Sebring & Ramsey 1996). There are also plans for future very large segmented telescopes (Ardeberg et al. 1996). It is therefore of great interest to determine the image quality degradation caused by segment misalignment.

The final image quality of a telescope depends on a large number of factors including aberrations inherent in the optical configuration and aberrations due to misalignment of the secondary mirror. The errors which are specific to a segmented telescope are those due to errors in the positioning of the segments. Each segment has three axial degrees of freedom; two degrees of rotation (tip and tilt) and axial position (piston). The lateral degrees of freedom of the segment are normally fixed to the primary mirror cell, but any errors in the lateral position give rise to figure errors. The segments will also undergo figure errors due to gravitational or thermal instabilities (as is the case with monolithic mirrors). Active optics may be used to control these errors, but the degree of control will be limited by noise and drift in the measurements of segment positions.

The image quality of astronomical telescopes is usually specified by demanding that the image width in the best *seeing* conditions be degraded by a small amount (e.g., 10%). The 'width' may be specified either as a full-width at half-maximum (FWHM) or the encircled energy diameter (EED) (D50 or D80). Another approach, different from these angular criteria, is to use the central intensity ratio (CIR), defined as the ratio between the peak of the image and that which would be obtained by an equivalent perfect telescope in the same *seeing* conditions. The usual design approach is to estimate the errors associated with each component of the telescope, and add them in quadrature. It should not be taken for granted that this approach is valid in the case of segmentation errors.

In order to analyze the effect of segmentation errors on the telescope modulation transfer function (MTF) we have developed analytical expressions for the simple case of a two-ring mirror (§ 2). We then examine their effect on image quality parameters (§ 3). The expressions are verified by numerical simulations and applied to a telescope with hexagonal segmentation.

2. SEGMENTED MIRROR MTF

The Modulation Transfer Function (MTF) and its Fourier Transform, the Point Spread Function (PSF), can be considered as fundamental measures of image quality. The MTF has the advantage that the complete system MTF is given by the product of the MTFs of the components of the system.

The MTF of a telescope in a vacuum, $M_{tel}(\nu)$, is given by the autocorrelation of the complex pupil transmittance $\Upsilon(r)$

$$M_{tel}(\nu) = \frac{1}{\pi(1-\varepsilon^2)} \int_S \Upsilon(|r|)\Upsilon^*(|r+\nu|)ds \ , \tag{1}$$

where ν is the normalized spatial frequency, r is the position in the pupil normalized to the radius of the pupil, ε the linear obscuration ratio and S the clear aperture. The complex transmittance inside the pupil, $\Upsilon(r)$, is defined by

$$\Upsilon(r) = \exp(ik\Delta(r)) \ , \tag{2}$$

where $\Delta(r)$ is the wavefront aberration function and $k = 2\pi/\lambda$.

Dierickx (1992) derives an expression for the MTF of an annular monolithic telescope assuming axisymmetrical wavefront errors, and employing a Taylor expansion of the MTF about spatial frequency zero;

$$M_{tel}(\nu) \simeq M_{tel}(0) + \frac{\nu}{1!}\frac{dM_{tel}}{d\nu}\bigg|_{\nu=0} + \frac{\nu^2}{2!}\frac{d^2M_{tel}}{d\nu^2}\bigg|_{\nu=0} + \frac{\nu^3}{3!}\frac{d^3M_{tel}}{d\nu^3}\bigg|_{\nu=0} \ . \tag{3}$$

It will be seen in § 3 that for long-exposure imaging, the effect of atmospheric turbulence is to drastically reduce the spatial cut-off frequency, and therefore an expansion about spatial frequency zero, will provide a good approximation for the MTF of the combined telescope-atmosphere system.

In order to investigate the effect of segmentation we assume a telescope with a primary mirror made up of two independent rings, with the boundary between the rings at radius ρ_I, and a linear obscuration ratio, ε. In this case the wavefront aberration function will be:

$$\Delta(\rho) = \begin{cases} \Delta_1(\rho) & \text{if} \quad \varepsilon \le \rho \le \rho_I \ , \\ \Delta_2(\rho) & \text{if} \quad \rho_I \le \rho \le 1 \ . \end{cases} \tag{4}$$

This choice of segmentation has the advantage of maintaining an axisymmetrical pupil, thus allowing the PSF to be calculated analytically using a Hankel transform (§ 3). This characterization of the pupil function allows us to simulate several types of wavefront errors; we refer to those errors specific to each ring as local

errors, while global errors are those which are continuous across the boundary between the rings (when there are no piston errors). This model supposes that the main effect of piston errors on image quality does not depend on where the piston errors occur; it will be shown using numerical simulations that in the case of a mirror made up of several segments, the rms piston error has the same effect as a single piston error in the two ring model (up to a certain value of piston error).

As a segmented pupil is employed, care must be taken in performing the pupil autocorrelation in order to properly handle the discontinuities in the pupil. In the case of a two-ring mirror, the integration in equation (1) can be divided into three zones. The first and third zones correspond to the regions where the first ring is correlated with the first ring of the shifted mirror, and where the second ring is correlated with the second ring of the shifted mirror, respectively. The second zone corresponds to the region where the first ring is correlated with the second ring of the shifted mirror.

For the monolithic case, Dierickx (1992) finds that aberrations have no effect on the first-order derivative of the MTF. However, in the presence of wavefront piston errors we find the following expression

$$\left.\frac{dM_{tel}(\nu)}{d\nu}\right|_{\nu=0} = -\frac{4}{\pi(1-\varepsilon^2)}\Big(1+\varepsilon+2\rho_I[1-\cos(k(\Delta_1(\rho_I)-\Delta_2(\rho_I))]\Big)\ . \tag{5}$$

This expression reduces to Dierickx's when the wavefront aberration function of the two rings is the same at the boundary ($\Delta_1(\rho_I) = \Delta_2(\rho_I)$). However, its validity is limited to $\varepsilon < \rho_1 < 1$, since when $\rho_1 = \varepsilon$ or $\rho_1 = 1$, the pupil autocorrelation integral contains two zones instead of three, and the third term of expression (5) disappears. This will be true for all derivatives of the MTF, and from here on, terms containing ρ_1 go to zero when $\rho_1 = \varepsilon$ or ρ_1=1. We will refer to the difference $\tau = (\Delta_1(\rho_I) - \Delta_2(\rho_I))$ as the piston error. This includes not only pure piston errors but also those due the segments having different figure errors.

The second-order derivative term in the absence of discontinuities is

$$\left.\frac{d^2M_{tel}(\nu)}{d\nu^2}\right|_{\nu=0} = -4\,\frac{k^2}{1-\varepsilon^2}\int_\varepsilon^1 \Delta'^2(\rho)\rho d\rho\ , \tag{6}$$

i.e., is proportional to the mean squared wavefront slope error ($\Delta'(\rho) = \frac{d\Delta(\rho)}{d\rho}$). In the presence of piston errors we find

$$\left.\frac{d^2M_{tel}(\nu)}{d\nu^2}\right|_{\nu=0} = -4\sigma^2 - \frac{4k\rho_I}{1-\varepsilon^2}[\Delta_1'(\rho_I)-\Delta_2'(\rho_I)]\sin(k\tau)\ , \tag{7}$$

where

$$\sigma^2 = \frac{k^2}{(1-\varepsilon^2)}\left(\int_\varepsilon^{\rho_I}\Delta_1'^2(\rho)\rho d\rho + \int_{\rho_I}^1 \Delta_2'^2(\rho)\rho d\rho\right)\ . \tag{8}$$

The second order effect of piston errors is zero if there are no figure errors. The discontinuity in the mirror has the same diffractive effect as the inner and outer edges of a monolithic mirror and like these, does not have a second order effect on the MTF. If there are figure errors, then the effect of piston is approximately linear (for small values of piston), and depends on the slope of the figure error at the boundary between the rings.

Finally, the third-order derivative is found to be given by

$$\begin{aligned}\left.\frac{d^3M_{tel}(\nu)}{d\nu^3}\right|_{\nu=0} &= \frac{4}{\pi(1-\varepsilon^2)}\Big(1+\frac{1}{\varepsilon}+\frac{2}{\rho_I}[1-\cos(k\tau)]\\ &+8k^2\Big(\varepsilon(\Delta_1'(\varepsilon))^2+\rho_I(\Delta_1'(\rho_I))^2+\rho_I(\Delta_1'(\rho_I))^2+(\Delta_2'(1))^2\Big)\\ &-\frac{16}{3}\rho_I k^2[(\Delta_1'(\rho_I))^2+\Delta_1'(\rho_I)\Delta_2'(\rho_I)+(\Delta_2'(\rho_I))^2]\cos(k\tau)\\ &-\frac{8}{3}k^2[\Delta_1'(\rho_I)-\Delta_2'(\rho_I)]\sin(k\tau)\\ &-\frac{16}{3}\rho_I k^2[\Delta_1''(\rho_I)-\Delta_2''(\rho_I)]\sin(k\tau)\Big)\ .\end{aligned} \tag{9}$$

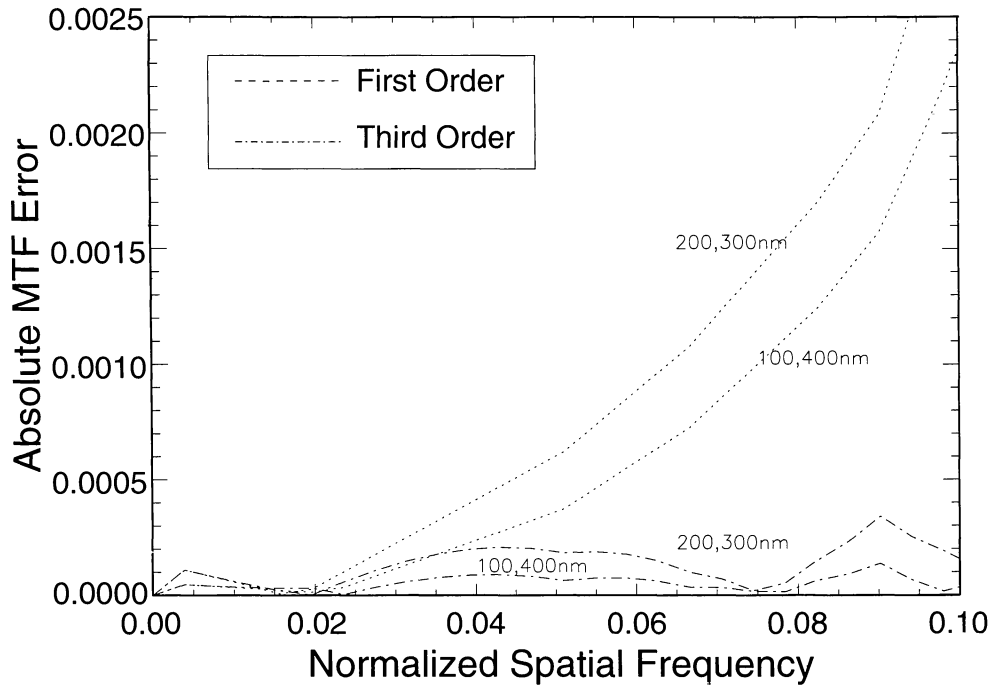

Fig. 1. Absolute MTF error between the simulated and predicted MTF for a two ring mirror for several values of piston errors. The numbers beside the curves indicate the values of piston rms error at the wavefront. The effect of 100nm and 200nm of piston error is found to be the same as the effect of 400nm and 300nm piston error, respectively. This is due to the symmetry of the effect around $\lambda/2$ (250nm).

The apparent singularity in equation (9) for $\varepsilon = 0$ is due to the fact that the derivation assumes $\varepsilon \geq \nu$. If this is not the case, then the integration limits have to be changed as the first ring does not intersect the first ring of the shifted mirror if $\varepsilon < \nu$, and in this case the terms containing ε disappear.

The expressions derived above have been checked by comparing with the results of numerical simulations of a two-ring mirror. In the simulations, the PSF is calculated by taking the squared modulus of the Fourier Transform of the simulated pupil function, and the MTF is obtained as the Fourier Transform of the PSF. This is faster than numerically computing the autocorrelation of the pupil function. Figure 1 shows the difference between the predicted and simulated MTF. In this figure we compare the simulation with the theoretical predictions for the MTF when the segments have piston errors alone. The difference is seen to be very small, indicating very good agreement between theoretical predictions and simulations.

3. IMAGE QUALITY WITH A SEGMENTED MIRROR

The quality of astronomical images may be measured using several parameters, including FWHM, EED (encircled energy diameter) (usually 50% [D50] and 80% [D80]) and the Central Intensity Ratio (CIR). For a *seeing* limited image, D50 = 1.08 FWHM, and D80 = 1.89 FWHM. It is usually required that a telescope does not degrade the best *seeing* conditions by more than a small amount (usually 10%) at visible wavelengths. The severity of this requirement depends strongly on the choice of image quality parameter. However, it appears that the D80 and the CIR parameters are the more useful since they determine the signal-to-noise ratio in the final image (Dierickx 1992).

We now assess the image quality parameters for the two-ring telescope model in the presence of atmospheric *seeing*. The results apply only to long-exposure images, i.e., to images recorded with exposure times much longer than the coherence time of atmospheric turbulence. The effect of *seeing* on the long-exposure image may be determined by multiplying the telescope MTF by an atmospheric MTF. If the *seeing* has Kolmogorov statistics then the atmospheric MTF is given by

$$MTF_{atmo}(\nu) = \exp[-(\frac{\nu}{\nu_0})^{\frac{5}{3}}] \,, \tag{10}$$

where

$$\nu_0 = \frac{r_0}{2.10\lambda} \text{ cycles/radian} ,$$

λ is the wavelength of observation and r_0 is the Fried parameter (Fried 1994). This parameter corresponds to a cut-off frequency introduced by the atmospheric turbulence. In the presence of *seeing* characterized by r_0, the angular resolution of a telescope of infinite diameter would be the same as that of a telescope of diameter r_0. For the simulations and theoretical calculations we have employed $\lambda = 500$nm and $r_0 = 0.2516$m (corresponding to a *seeing* value of 0.4 arcsec). For a telescope of diameter 10m, the corresponding cut-off frequency is 0.0146 times the diffraction-limited value.

As already stated, the PSF can be obtained by taking a Fourier Transform of the MTF. Since the MTF is axially symmetric, the two-dimensional Fourier Transform can be replaced by a one-dimensional Hankel Transform,

$$PSF(r) = 8 \int_0^1 M(\nu) J_0(2\pi r\nu) \nu d\nu , \tag{11}$$

where J_0 is the zero-order Bessel function, r the image radius in units of λ/D and $M(\nu) = MTF(\nu)_{tel} \times MTF(\nu)_{atmo}$. For $\zeta = D/r_0$ sufficiently large ($\zeta > 20$), the integration can be extended to the interval from 0 to ∞ since $M(\nu)$ converges rapidly to zero. It is then possible to establish a series approximation for the PSF, as described by Dierickx (1992). The encircled energy can also be determined by numerical integration of this analytical expression for the PSF.

We have derived the PSF and encircled energy as series approximations for our two-ring model. In the case of the CIR it is possible to find an analytical expression. Using the series expansion for the PSF and the definition of the CIR we can develop a third-order approximation. The expression is quite long for local errors; here we present the expression for global figure errors and piston errors alone

$$CIR = 1 - \frac{4}{\pi\beta}[2\rho_I b_0 \zeta - \frac{d_0}{3\zeta\rho_I}](1 - \cos(k\tau)) + \frac{2c_0}{\beta}\sigma^2$$
$$- \frac{16 d_0}{3\pi\zeta\beta}[\varepsilon(\Delta'(\varepsilon))^2 + (\Delta'(1))^2] - \frac{32 d_0}{3\pi\zeta\beta}[\rho_1(\Delta'(\rho_I))^2(1 - \cos(k\tau))] , \tag{12}$$

where we define,

$$\beta = \zeta^2(1-\varepsilon^2)[1 - \frac{1}{\zeta(1-\varepsilon)}(4b_0 - \frac{2d_0}{3\zeta^2\varepsilon})] , \tag{13}$$

and $b_0 = 0.483197$, $c_0 = 0.306969$, $d_0 = 0.235430$.

The formula for the CIR may be understood by identifying each term individually; the first term comes from the first and third order expansion of the piston error alone, the second is a second order expansion of the figure errors and is independent of piston errors. The third term arises from the third-order expansion of the figure errors. The fourth comes from the third-order expansion of both piston and figure errors, and is non-zero only when both piston and figure errors are non-zero.

The cross terms in the formula imply that there are some cross effects between different errors at the mirror. It is, therefore, not true in general that piston errors and figure errors can be added quadratically in order to find the final effect on the image. It has been suggested (Dierickx 1994) that the effective CIR due to the combination of different errors may be found by combining CIRs due to each error, CIR_n, according to the formula

$$CIR \approx 1 - \sum_n (1 - CIR_n) . \tag{14}$$

However, this formula will not be valid when the cross-terms are important. This is shown in Figure 2 where we show the CIR corresponding to a combination of defocus and piston error. Crosses represent the

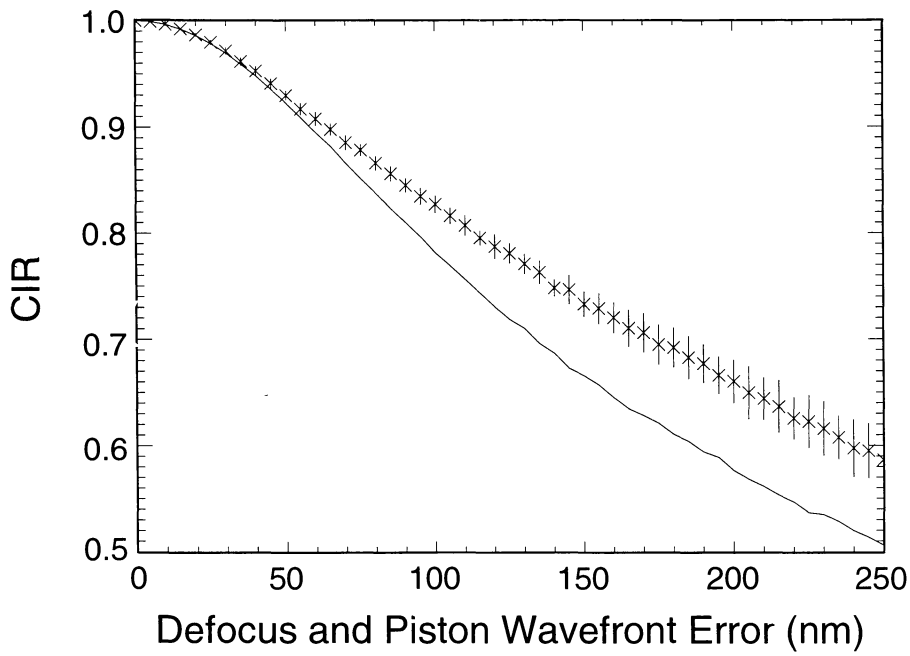

Fig. 2. The central intensity ratio (CIR) as a function of wavefront piston and defocus errors for a 36-segment mirror. The crosses represent the data obtained from simulations when both defocus and piston errors are present, and the continuous line represents an estimation for the CIR employing equation (14). It can be seen that the prediction from equation (14) is rather pessimistic in this case and cross-terms between aberrations can have an important contribution to the CIR value.

results obtained from simulations when both aberrations are present. The continuous line represents the CIR obtained by application of equation (14).

When there are only piston errors, the formula for the CIR reduces to the simple expresion:

$$CIR = 1 - \alpha[1 - \cos(k\tau)] \ , \tag{15}$$

where

$$\alpha = \frac{4}{\pi\beta}[2\rho_I b_0 \zeta - \frac{d_0}{3\zeta\rho_I}] \ , \tag{16}$$

which depends only on the radius of the discontinuity, ρ_1, and the ratio between the diameter of the telescope and r_0.

The values for the CIR calculated numerically for a two-ring telescope have been compared with those obtained from the theoretical approximation, with D = 10m, ρ_I = 0.5 in an atmosphere characterized by r_0=0.2516m at $\lambda = 0.5\mu$m. The results are shown in Figure 3. The agreement is seen to be quite good. The non-monotonic behaviour seen in this figure is due to the symmetry of the problem around $\lambda/2$. When the wavefront piston error τ, is equal to a whole wavelength, the situation is indistinguishable from having zero wavefront piston error, and the CIR is therefore unity.

Analytical expressions or series approximations cannot be obtained for the parameters based on angular criteria, FWHM, D50 and D80. As theoretical predictions for their values we have employed values interpolated from the series expansions for the PSF and encircled energy. We find that in the case of piston errors alone, they depend on the piston errors in the same way as the CIR, i.e., (FWHM, D50, D80) $\propto \gamma + \delta(1 - \cos(k\tau))$.

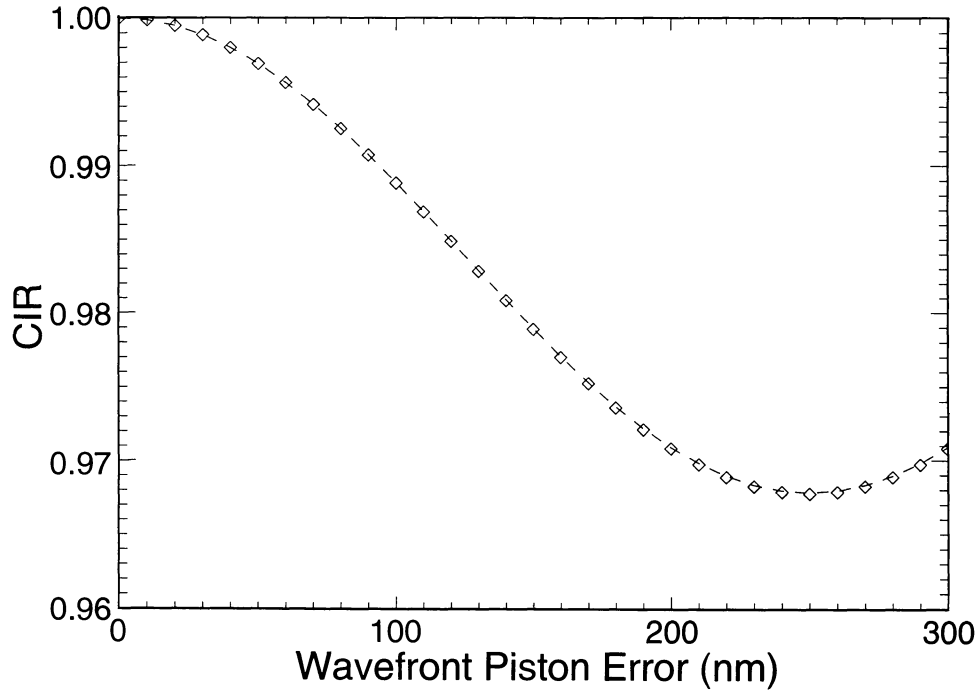

Fig. 3. The central intensity ratio (CIR) as a function of wavefront piston errors for a two ring mirror. The squares represent the simulated data and the theoretical prediction is given by the dashed line.

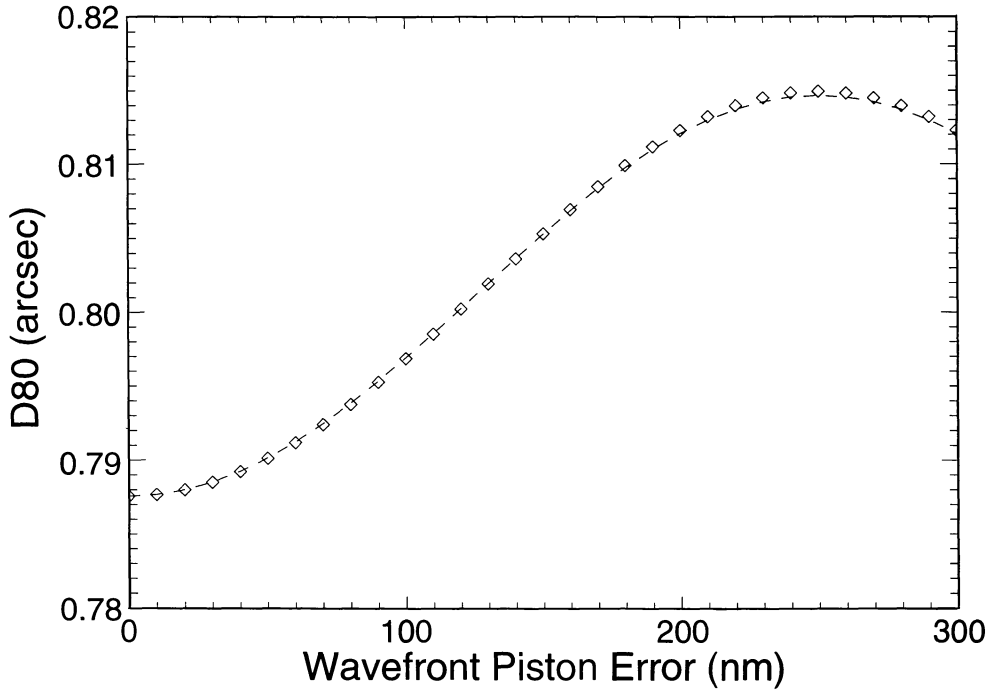

Fig. 4. The 80% encircled energy diameter (D80) as a function of wavefront piston errors (τ) for a two ring mirror. The squares represent the simulated data and a fit of the form D80 = $\beta + \gamma(1 - cos(k\tau))$ is given by the dashed line, where β and γ are parameters of the fit.

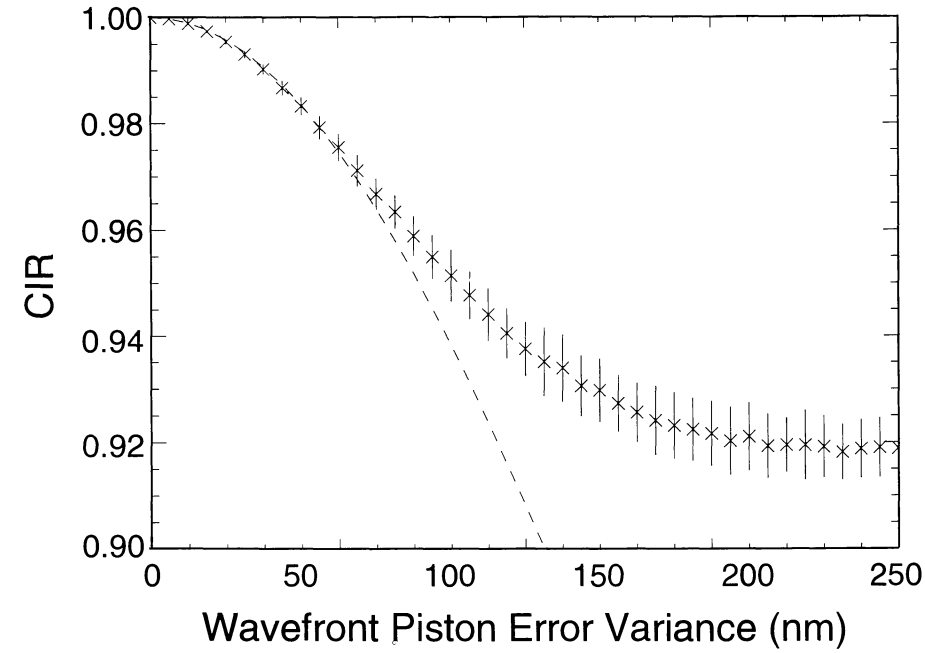

Fig. 5. The central intensity ratio (CIR) as a function of wavefront piston errors (τ) for a 36-segment mirror. The crosses represent the simulated data and the dashed line represents the fit to the expression: CIR $= 1 - \alpha'[1 - \cos(k\tau)]$ (α' is the parameter of the fit), for piston errors less than 80nm.

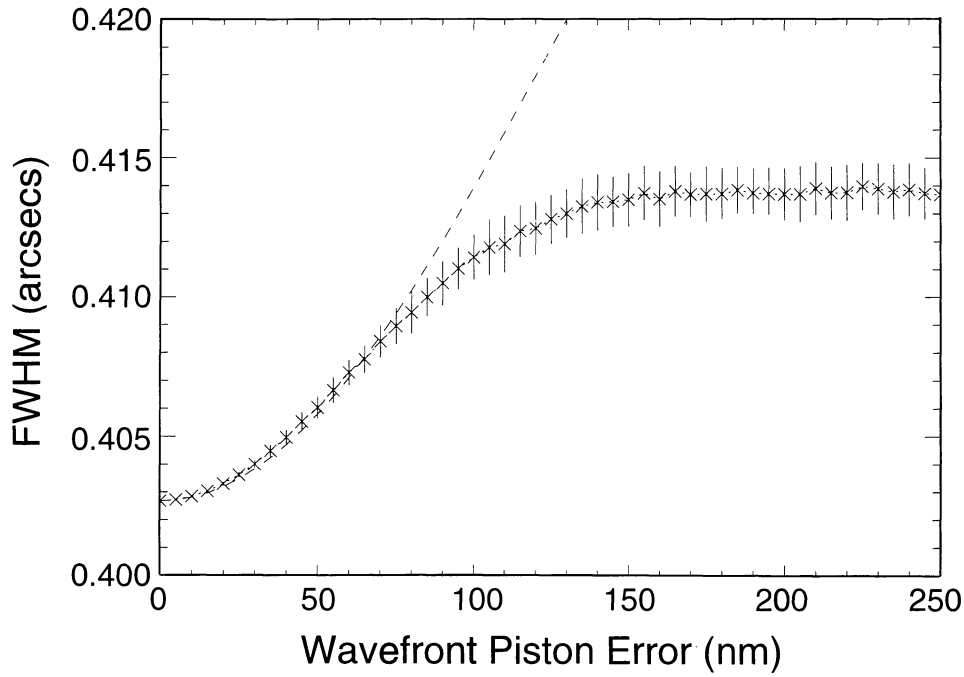

Fig. 6. The full width half maximum (FWHM) as a function of wavefront piston errors (τ) for a 36-segment mirror. The crosses represent the simulated data and the dashed line represents the fit to the expression: FWHM $= \beta - \gamma[1 - \cos(k\tau)]$, for piston errors less than 80nm, where β and γ are parameters of the fit.

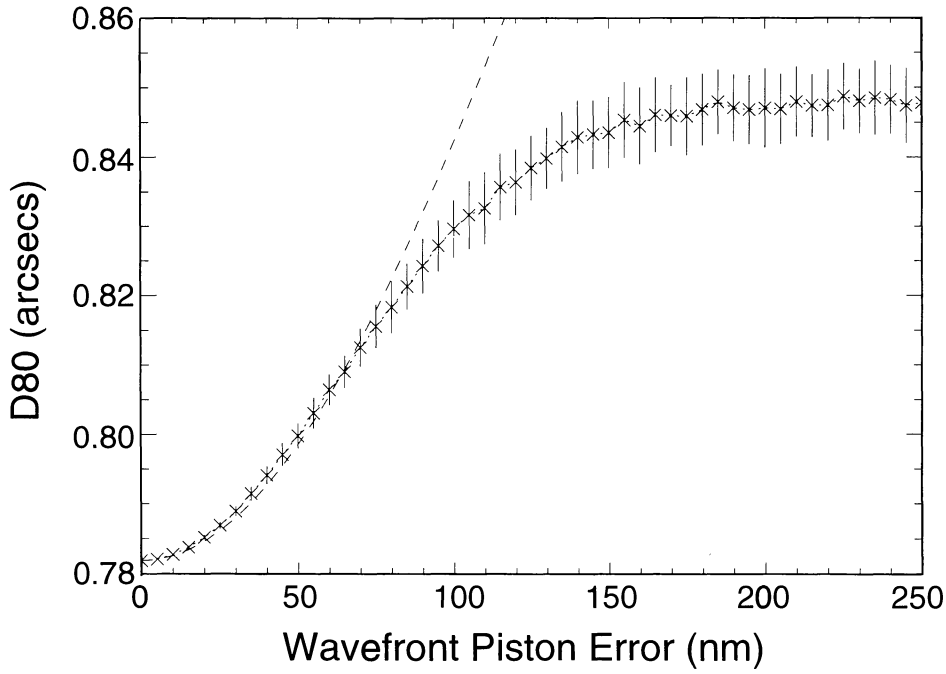

Fig. 7. The 80% encircled energy diameter (D80) as a function of wavefront piston errors (τ) for a 36-segment mirror. The crosses represent the simulated data and the dashed line represents the fit to the expression: D80 $= \beta - \gamma[1 - \cos(k\tau)]$, for piston errors less than 80nm, where β and γ are parameters of the fit.

Figure 4 shows the behaviour of the $D80$ parameter when there are piston errors alone, and a fit of the form $\gamma + \delta(1 - \cos(k\tau))$ for these values.

We have carried out simulations of a mirror made up of 36 hexagonal segments in order to check that the results of our simple model are useful for more realistic geometries. The geometry is the same as that employed in the Keck telescopes. Figure 5 shows the results obtained from simulations where the only error introduced is piston errors in the individual segments. The dashed line shows a fit of the form $1 - \alpha'[1 - \cos(k\tau)]$, as derived from our model. The agreement is seen to be quite good for piston errors below $\approx$ 80nm. Beyond this value, our model would predict an increase in CIR, but the large number of randomly pistoned segments in the more realistic geometry prevents this from happening. Nevertheless, phasing techniques such as those employed at the Keck telescopes allow large segmented telescopes to operate in the regime of validity of our approximation.

4. CONCLUSIONS

We have analyzed the effect of segmentation errors using a two-ring mirror, obtaining approximations for the MTF, PSF, encircled energy and the CIR. When the only error is piston, the effect is similar to the effect of diffraction at the inner and outer edges of the pupil, and appears in first and third order expansions of the MTF. Figure errors alone appear in second order. If both piston and figure errors are present then cross-terms arise due to the effective piston error introduced between the segments by the figure errors.

These results have been compared with those obtained from simulations, and show very good agreement.

The functional dependence of the image quality parameters (CIR, FWHM, D50, D80) on piston and figure errors has been established, and we find a dependence of the form $\gamma + \delta(1 - \cos(k\tau))$ for piston errors. When piston and figure errors are combined, the image quality parameters show a cross-term contribution from both types of errors.

These results have been applied to segmented mirrors with hexagonal segmentation; for a mirror composed of 36 hexagonal segments the functional form of the effect of piston errors in the image quality parameters

(CIR, FWHM, D50, D80) is found to be the same as for a two-ring telescope for piston errors less than $\approx$ 80nm when λ = 500nm, (Figures 5, 6, and 7). The combined effect of having a parameter dependence of the form $\gamma + \delta(1 - \cos(k\tau))$ together with having a large number of segments and thus of discontinuities, causes the image quality parameters to reach a constant lower limit. However, for large piston errors the defocus of the segments will cause the CIR and the other image quality parameters to degrade further.

REFERENCES

Ardeberg, A., Andersen, T., Owner-Petersen, M., & Jessen, N.-C. 1996, in Optical Telescopes of Today and Tomorrow, Proc. Soc. Photo-Opt. Instrum. Eng., ed. A. Ardeberg, 2871, 585

Dierickx, P. 1992, J. of Modern Optics, 39, 569

_____. 1994, in Advanced Technology Optical Telescopes V, Proc. Soc. Photo-Opt. Instrum. Eng., ed. L. M. Stepp, 2199, 950

Fried, D. L. 1994, in Adaptive Optics in Astronomy, ed. D. M. Alloin & J-M. Mariotti (Dordrecht: Kluwer), 25

Nelson, J. E., & Gillingham, P. 1994, in Advanced Technology Optical Telescopes V, Proc. Soc. Photo-Opt. Instrum. Eng., ed. L. M. Stepp, 2199, 82

Sebring, T. A., & Ramsey, L. W. 1996, in Optical Telescopes of Today and Tomorrow, Proc. Soc. Photo-Opt. Instrum. Eng., ed. A. Ardeberg, 2871, 32

Carmen Dolores Bello: Instituto de Astrofísica de Canarias, Calle Vía Láctea s/n, 38200 La Laguna, Tenerife, Spain (cbello@ll.iac.es).

Javier Castro and Nicholas Devaney: Gran Telescopio Canarias Project Office, 38200 La Laguna, Tenerife, Spain (jcl,ndevaney@ll.iac.es).